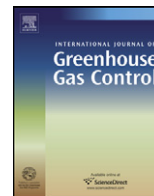




Contents lists available at SciVerse ScienceDirect

International Journal of Greenhouse Gas Control

journal homepage: www.elsevier.com/locate/ijggc

Complex evolution of coal permeability during CO₂ injection under variable temperatures

Hongyan Qu^a, Jishan Liu^{a,*}, Zhongwei Chen^a, Jianguo Wang^a, Zhejun Pan^b, Luke Connell^b, Derek Elsworth^c

^a School of Mechanical and Chemical Engineering, The University of Western Australia, WA 6009, Australia

^b CSIRO Earth Science and Resource Engineering, Private Bag 10, Clayton South, Victoria 3169, Australia

^c G³ Center, EMS Energy Institute, and Energy and Mineral Engineering, Pennsylvania State University, University Park, PA, USA

ARTICLE INFO

Article history:

Received 13 December 2011

Received in revised form 11 April 2012

Accepted 11 April 2012

Keywords:

Coal permeability

Gas sorption

Local swelling

Global swelling

Thermal impact

ABSTRACT

Although the influence of cross couplings between coal deformation, gas flow and thermal transport has been widely recognized, their impacts on the evolution of coal permeability are still not well understood. CO₂ may be injected at -40°C , 60°C lower than that of the targeted coal seams for sequestration. Under these injection conditions, coal matrix may swell due to the thermal expansion and shrink due to the change in adsorption capacity. This uncertainty of swelling/shrinking complicates the prediction of coal permeability. In this study, a fully coupled coal deformation, gas flow and transport, and thermal transport model is developed to evaluate the complex evolution of coal permeability under the combined influence of variable gas pressure and temperature. These combined effects are evaluated through explicit simulations of the dynamic interactions between coal matrix swelling/shrinking and fracture aperture alteration, and translations of these interactions to the evolution of coal permeability. The fully coupled model is applied to evaluate why coal permeability changes instantaneously from reduction to enhancement under the free swelling condition as widely reported in the literature. Our results have revealed the transition of coal matrix swelling from local swelling to macro-swelling as a novel mechanism for the simultaneous switching of coal permeability from the initial reduction to the late recovery. At the initial stage of CO₂ injection under variable temperatures, matrix swelling due to gas sorption, thermal expansion and the change in adsorption capacity is localized within the vicinity of the fracture compartment. As the injection continues, the swelling zone is widening further into the matrix and the swelling becomes macro-swelling. When the swelling is localized, coal permeability is controlled by the internal fracture boundary condition and behaves volumetrically; when the swelling becomes macro-swelling, coal permeability is controlled by the external boundary condition.

© 2012 Elsevier Ltd. All rights reserved.

1. Introduction

CO₂ injection into coal seams triggers complex interactions between coal and fluids. These include gas adsorption and its associated coal swelling, coal porosity change and permeability modifications. Among which, adsorption-induced coal matrix swelling is the leading issue due to its dominant effect on the coal permeability as CO₂ flows through the cleats and diffuses to the coal matrix. A comprehensive understanding of these interactions is essential for the successful enhanced coalbed methane (ECBM) production and CO₂ storage in coal seams under particular in situ pressure and temperature conditions.

A number of experimental and numerical studies have been performed to predict the permeability change during CO₂ geological

sequestration under isothermal conditions. Laboratory measured coal permeability to adsorbing gases such as CH₄ and CO₂ is lower than that to non-adsorbing or lightly adsorbing gases such as argon and nitrogen (N₂) (Chen et al., 2011; Siriwardane et al., 2009; Somerton et al., 1975). Under constant temperature and total stress, permeability decreases with the increase of pore pressure due to coal swelling (Mazumder and Wolf, 2008; Pan et al., 2010; Robertson, 2005; Wang et al., 2010, 2011), and increases with the decrease of pore pressure due to matrix shrinkage (Cui and Bustin, 2005; Harpalani and Chen, 1997; Harpalani and Schraufnagel, 1990; Seidle and Huitt, 1995). The decrease of permeability is found to be as much as five orders of magnitude as the confining pressure is in the range of 0.1–70 MPa (Durucan and Edwards, 1986; Somerton et al., 1975).

According to the field and laboratory observations, various coal permeability models have been proposed on the basis of poroelasticity for some idealized coal structure as well as specific conditions. A widely used theoretical permeability model was derived by

* Corresponding author.

E-mail address: jishan@cyllene.uwa.edu.au (J. Liu).

Nomenclature

p	gas pressure within the system
T	temperature within the system
α_T	the coefficient of volumetric thermal expansion
ε_{ij}	component of total strain tensor
σ_{ij}	component of total stress tensor
ε_s	sorption-induced volumetric strain
K	bulk modulus of coal
G	shear modulus of the coal
E	equivalent Young's modulus
α	Biot coefficient
δ_{ij}	Kronecker delta with 1 for $i=j$ and 0 for $i \neq j$
ε_g	the proportional ratio of sorption-induced volumetric strain to sorption volume
V_s	adsorption volume
V_L	Langmuir volume
p_L	Langmuir pressure
ρ_g	density of free phase gas
$\vec{\mu}$	Darcy velocity vector
Q_s	gas source or sink
D	molecular diffusion coefficient
m	gas content
ρ_{ga}	gas density at standard conditions
ρ_c	coal density
ϕ	coal porosity
M_g	molar mass of the gas
R	universal gas constant
Z	compressibility factor
k	micor pore permeability
k_f	cleat permeability
k_{f0}	initial cleat permeability
k_{fi}	cleat permeability for i direction
b_j	fracture aperture for i direction
s	fracture spacing
ν	fluid viscosity
∇p	fluid pressure gradients
ϕ_0	initial porosity
ε_e	effective volumetric strain
ε_v	total volumetric strain
p/K_s	compressive strain
K_s	bulk modulus of coal grains
ε_T	thermal volumetric strain
d_e	effective diameter of grains
C_{eq}	effective volumetric heat capacity
K_{eq}	effective thermal conductivity
C_L	volumetric heat capacity of the moving fluid
Q_H	general heat source
Q_G	geothermal heat source
N	heat flux vector
H	enthalpy of the system
q	energy added to the system through heat
C_p	heat capacity at constant pressure
μ_{JT}	Joule–Thomson coefficient

Palmer and Mansoori (1996), who defined permeability as a function of effective stress and matrix shrinkage. Shi and Durucan (2004a,b) presented a cleat permeability model for gas-desorbing coalbeds under uniaxial strain conditions where the changes in the cleat permeability were assumed to be controlled by the prevailing effective horizontal stresses normal to the cleats. Following the above work, Cui and Bustin (2005) quantitatively studied the effects of reservoir pressure and sorption-induced volumetric strain on

coal-seam permeability and derived a stress-dependent permeability model.

Since the above matchstick coal models were derived on the assumption that the matrix blocks are completely separated from each other in a stacked structure, permeability should not change under conditions of constant confining stress (Liu and Rutqvist, 2010; Liu et al., 2011a). However, this interpretation is not consistent with laboratory observations (Harpalani and Chen, 1997; Pan et al., 2010; Pini et al., 2009), where dramatic reduction in permeability was shown with the injection of gas. It was attributed to the swelling of the matrix bridges which connect coal matrix blocks to each other (Liu and Rutqvist, 2010). A new coal permeability model was developed associated with internal swelling stress to incorporate the fracture–matrix interaction. The ignorance of the internal actions between coal fractures and matrix may be an alternate reason (Liu et al., 2010b, 2011a).

Even though a large variety of coal permeability models have been proposed, these permeability models were derived based on assumptions that the temperature of the injected CO₂ is the same as that in coal seams and it remains unchanged during the injection and adsorption processes. However, in most field injection sites, CO₂ is commonly injected into coal at –40 °C to –20 °C at liquid phase or over 30 °C at supercritical phase while the initial temperature of coal seams normally ranges from 27 °C to 52 °C. In such a case, the injection of CO₂ yields significant temperature discrepancy between the injected fluid and coal seams. This contrast in temperature can change the physical, chemical and thermal state of subsurface formation and break the pre-existing equilibrium condition. Similar to the effect of pressure, temperature has considerable impact on gas adsorption and coal permeability as well, which may accelerate or delay permeability switch from reduction to recovery by enhancing or reducing the magnitude of swelling/shrinkage of cleats and matrix.

Several experiments have been conducted to investigate the temperature evolution and its effect on coal properties during the CO₂ injection. The classical Joule–Thomson experiment was focused on the cooling effect on gas injectivity. It was found that temperature can drop over 20 °C due to gas expansion, which has negative effect on permeability and injectivity (Oldenburg, 2007). Long et al. (2009) measured the permeability change under different temperatures by injecting N₂, CH₄ and CO₂ into coal samples. Their results showed that the temperature variation has a major impact on coal permeability.

There is a general agreement that the rate of sorption of CO₂ and CH₄ strongly depend on pressure and temperature. Experiments on CO₂ sorption kinetics performed on dried coal at the equilibrium temperature between 10 °C and 60 °C showed that the adsorption rate of CO₂ is positively correlated with temperature, and an increase in pressure and temperature causes a decrease in equilibrium time (Charrière et al., 2010). Similar results were reported by Deishad et al. (2009), who found that equilibration time decreases with increasing temperature due to the increase of diffusion rate.

While adsorption rate controls the equilibrium time, adsorption capacity determines the magnitude of swelling and shrinkage (Pan and Connell, 2007; Qu et al., 2010). It was found that adsorption rate increases with increasing temperature, but the effect of temperature on sorption capacity is highly related to coal ranks. The thermal experiment for the coal of low ranks shows that temperature plays an insignificant role in storage capacity because absolute differences between all the isotherms are found to be small (Crosdale et al., 2008). However, for the coal of high ranks, it has been found that adsorption capacity decreases significantly with increasing temperature (Saunders and Yang, 1985; Krooss et al., 2002). The same conclusion was drawn in the experimental data from sorption curves of three dry Argonne Premium coals, for N₂, CH₄ and CO₂ at two different temperatures (Sakurovs et al., 2008).

Furthermore, similar results were found for bituminous coals by a number of authors (Levy et al., 1997). These observations are inconsistent with the results of Langmuir gas sorption models (Donald, 1978), which predict that the sorption capacity is independent of temperature. Even though the Langmuir pressure p_L (Lama and Bodziony, 1996) was found to decrease with increasing temperature (Pini et al., 2009) and vary as a function of rank (Crosdale et al., 2008), the temperature dependency of Langmuir pressure has not been incorporated into gas sorption and coal permeability models.

Based on the experiment results and field observations, a few models have been presented to define the relationship between permeability variation and temperature change. Elsworth (1989) developed a conceptual model that described permeability enhancement subjected to temperature changes. This study demonstrated that thermal diffusion between solid and fluid phases is an important process that could change permeability significantly even under relatively modest temperatures. Zhou et al. (1998) developed a thermoporoelastic model taking into account the coupled thermo-hydro-mechanical effects. They found that changes in stresses, hydraulic gradient, and temperature gradient can cause permeability to change. However, these models could not be applied to coal since no adsorption effect is considered on rock.

In spite of the effect on adsorption capacity, temperature impacts permeability via thermal expansion as well. Thermal expansion caused by high temperature injection leads coal matrix and cleats to swell. Permeability is primarily determined by the cleat aperture (Wu et al., 2010a,b; Zhang et al., 2008). The change in cleat aperture is a function of effective stress through poroelasticity, but coal swelling and shrinkage under a confining stress may also change the cleat aperture (Izadi et al., 2011; Wu et al., 2010a,b). Thus, the net change in coal permeability is a function of both the poroelastic response and the coal swelling or shrinkage.

Over the past few years, a series of advanced modelling tools have been developed to quantify the complex coal–gas interactions (Zhu et al., 2011; Chen et al., 2010a,b; Connell, 2009; Connell and Detournay, 2009; Gu and Chalaturnyk, 2005a,b, 2006; Liu et al., 2010a,b; Wu et al., 2010a,b, 2011; Zhang et al., 2008). These works have provided a coupling approach to represent important non-linear responses of coal matrix to the effective stress effects.

In our previous study (Liu et al., 2011b), we found the transition of coal matrix swelling from local swelling (internal fracture controlled) to global-swelling (external boundary controlled) as a novel mechanism for coal permeability switching from reduction to enhancement under the influence of gas sorption. Our major findings include: (1) at the initial stage of CO₂ injection, matrix swelling is localized within the vicinity of the fracture compartment. As the injection continues, the swelling zone is extending further into the matrix and becomes macro-swelling; (2) matrix swelling processes control the evolution of coal permeability. When the swelling is localized, coal permeability is controlled by the internal fracture boundary condition and behaves volumetrically; when the swelling becomes macro-swelling, coal permeability is controlled by the external boundary condition and behaves non-volumetrically; and (3) matrix properties control the switch from local swelling to macro swelling and the associated switch in permeability behaviour from reduction to recovery. This study extends this modelling approach to evaluate the comprehensive thermal effect on the coal permeability during CO₂ injection and predict the permeability switch from reduction to recovery under variable temperatures. The model formulation is based on our previous work (Zhu et al., 2011). In our new formulations, we include the influence of temperature on sorption capacity via the temperature dependent Langmuir pressure and modify the conventional Langmuir adsorption equation. The effect of thermal stress, thermal expansion on permeability and the effect of temperature on coal matrix swelling are taken into account and coupled with gas

flow and coal deformation. Permeability is also investigated with respect to the adsorption amount to reflect the permeability evolution during the dynamic adsorption process.

2. Formulation of coupled processes

When coal is recovered by mining, or fluid recovered or injected, complex interactions of stress and flow have strong influences on gas sorption, coal deformation, porosity and permeability change. In this study, we define these interactions as ‘coupled processes’ implying that one physical process affects the initiation and progress of another. The individual process, in the absence of full consideration of cross couplings, forms the basis of very well-known disciplines such as elasticity, hydrology and heat transfer. Therefore, the inclusion of cross couplings is the key to rigorously formulate the full mechanism of coal–gas interactions.

In this section, a set of non-isothermal governing equations is developed for deformable coal medium, starting with appropriate local formulation expressing the balance law of continuum mechanics, coupled with mass and energy conservation laws, as well as gas flow and transport equation. The mass balance equation is employed to describe the microscopic behaviour of gas with heat transport. Macroscopic mass transport is obtained through the gas flow equations incorporated with porosity and permeability models. The fluid properties like viscosity and density are defined as a function of temperature, and the effect of temperature on the gas adsorption and thermal expansion is taken into account through the Langmuir coefficient and Joule–Thomson process. The governing field equations are solved to obtain the general field variables like reservoir pressure and temperature and to predict the effect of temperature on the coal porosity and permeability change during the CO₂ injection and adsorption processes.

2.1. Coal deformation

The stress–strain relationships for a thermo-elastic porous medium can be easily tracked in the literature (Bear and Corapcioglu, 1981; Nowacki, 1995). In this section, the stress–strain relationships for a non-isothermal linear elastic porous medium are derived, where an analogy is applied between thermal contraction and matrix swelling/shrinkage associated gas adsorption/desorption in coalbeds. The coal mass expands as the temperature increases, including both the solid phase and the fluid phase in pores and fractures, leading to a potential change of the porosity and permeability of the coal mass. In such a case, thermal effect can directly be analogous to the effect of effective stress, where matrix porosity changes as pore pressure varies. Assuming thermal expansion/contraction and matrix swelling/shrinkage are isotropic, the stress–strain relationships for a non-isothermal coalbed may be written as

$$\Delta \varepsilon_{ij} = \frac{1}{2G} \Delta \sigma_{ij} - \left(\frac{1}{6G} - \frac{1}{9K} \right) \Delta \sigma_{kk} \delta_{ij} + \frac{\alpha}{3K} \Delta p \delta_{ij} + \frac{\Delta \varepsilon_s}{3} \delta_{ij} + \frac{\alpha_T}{3} \Delta T \delta_{ij} \quad (1)$$

ε_{ij} represents the component of total strain tensor; σ_{ij} denotes the component of total stress tensor; ε_s is the sorption-induced volumetric strain. E is the equivalent Young’s modulus of the coal-fracture assemblage; K represents the bulk modulus of coal; G is the shear modulus of the coal. p is the gas pressure and T is temperature within the system. δ_{ij} is the Kronecker delta with 1 for $i=j$ and 0 for $i \neq j$. α is the Biot coefficient; α_T is the coefficient of volumetric thermal expansion incorporating those of both solid phase and the fluid phase. However, the thermal strain induced by the expansion/contraction of the fluid phase is usually neglected since

the thermal expansion coefficient of the fluid phase is relatively small in comparison with that of the solid phase.

For a system containing a single gas phase, the sorption-induced volumetric strain ε_s is usually represented by a Langmuir type function (Harpalani and Schraufnagel, 1990; Cui and Bustin, 2005; Robertson and Christiansen, 2007), defined as

$$\varepsilon_s = \varepsilon_L \frac{p}{p_L(T) + p} \quad (2)$$

where ε_L is the Langmuir-type matrix swelling/shrinkage coefficient and p_L is the Langmuir pressure, representing the maximum swelling capacity and the pore pressure at which the adsorption volume is half of the maximum adsorption volume, respectively. Both parameters are temperature related, and p_L is defined in Section 2.5.1.

Volumetric strain associated with gas sorption can also be measured in terms of the adsorbed gas volume at standard pressure and temperature. Experiments on the volumetric strain associated with methane and carbon dioxide adsorption have shown that the sorption-induced volumetric strain is approximately proportional to the volume of adsorbed gas (Cui and Bustin, 2005; Clarkson and Bustin, 2010), which also has been confirmed by Day et al. (2010). The relationship is described as

$$\varepsilon_s = \varepsilon_g V_s \quad (3)$$

where ε_g is the proportional ratio of sorption-induced volumetric strain to sorption volume; V_s is the sorption volume.

A modified Langmuir volume equation is established to describe the sorption volume for CO₂.

$$V_s = V_L \frac{p}{p_L(T) + p} \quad (4)$$

where V_L is the Langmuir volume.

The matrix swelling is proportional to the volume of gas adsorbed, and the amount of adsorbed gas is related to the pressure by Langmuir equation. Then the relationship between swelling and pressure as well as temperature can be written as:

$$\varepsilon_s = \varepsilon_g V_s = \varepsilon_g V_L \frac{p}{p + p_L(T)} \quad (5)$$

2.2. Gas flow and transport

Gas transport in coal seams commonly accommodates two serial transport mechanisms: diffusion through the coal matrix and laminar flow through the cleat system (Bai and Elsworth, 2000; Elsworth and Bai, 1992).

The gas transport equation including gas advection and diffusion mechanisms for a single component gas is defined as

$$\frac{\partial m}{\partial t} + \underbrace{\nabla \cdot (\rho_g \cdot \vec{\mu})}_{\text{advection}} + \underbrace{\nabla \cdot (-D \nabla m_a)}_{\text{diffusion}} = Q_s \quad (6)$$

$$m = m_f + m_a, \quad m_a = (1 - \phi) \rho_{ga} \rho_c \frac{V_L p}{p + p_L}, \quad m_f = \rho_g \phi \quad (7)$$

where ρ_g is the density of free phase gas, $\vec{\mu}$ is the Darcy velocity vector and Q_s is the gas source or sink. D is the molecular diffusion coefficient. m is the gas content including both free-phase content m_f and adsorbed content m_a ; ρ_{ga} is the gas density at standard conditions; ρ_c is the coal density and ϕ is coal porosity. V_L represents the Langmuir volume constant. According to the real gas law, gas density varies with pressure and temperature, which is proportional to the pore gas pressure and inversely proportional to temperature and can be described as

$$\rho_g = \frac{M_g}{ZRT} p \quad (8)$$

where M_g is the molar mass of the gas, R is the universal gas constant, and Z is the compressibility factor that accounts for the non-ideal behaviour of the gas.

The linear momentum balance equation can be expressed in the form of Darcy's law. Assuming the effect of gravity is relatively small and can be neglected, the Darcy velocity may be defined as

$$\vec{\mu} = -\frac{k}{\nu} \nabla p \quad (9)$$

where $\vec{\mu}$ is the Darcy velocity; k is the micro pore permeability; ν is the fluid viscosity; ∇p is the fluid pressure gradients.

Gas flows into the cleats from the injection well and then diffuses through the coal matrix and adsorbs on the internal surface of the pores. The diffusion process is caused by random molecular motions and controlled by the molecular diffusion coefficient D . It is reasonable to expect that the gas diffusion in the coal matrix is affected by the characteristics of adsorption, gas molecular geometry, and coal pore structure, which will not be discussed in this paper.

2.3. Coal permeability

The coal porosity ratio changes with the effective strain increment as (Liu et al., 2010a),

$$\frac{\phi}{\phi_0} = 1 + \frac{\alpha}{\phi_0} \Delta \varepsilon_e \quad (10)$$

where ϕ_0 is the initial porosity; ε_e is the effective volumetric strain, and its increment is defined as

$$\Delta \varepsilon_e = \Delta \varepsilon_v + \frac{\Delta p}{K_s} - \Delta \varepsilon_s - \Delta \varepsilon_T \quad (11)$$

where ε_v is total volumetric strain; p/K_s is the compressive strain; K_s represents the bulk modulus of coal grains; ε_T is the thermal volumetric strain.

The relationship between the porosity, permeability and the grain-size distribution in porous media has been defined as (Chilingar, 1964)

$$k = \frac{d_e^2 \phi^3}{72(1 - \phi)^2} \quad (12)$$

where d_e is the effective diameter of grains.

If the porosity is much smaller than 1 (normally less than 10%), the cubic relationship between permeability and porosity is yielded as

$$\frac{k}{k_0} = \left(\frac{\phi}{\phi_0} \right)^3 \quad (13)$$

Substituting Eq. (10) into Eq. (13), changes in coal permeability are determined by the redistribution of effective stress or strain due to varied conditions such as gas injection.

$$\frac{k}{k_0} = \left[1 + \frac{\alpha}{\phi_0} \Delta \varepsilon_e \right]^3 \quad (14)$$

2.4. Thermal transport

To understand the CO₂ injection induced coal-fluid interactions, thermal processes need to be evaluated. The evolution of the local temperature depends on several factors such as the enthalpy of the injected CO₂, the heat capacity and heat conductivity of the formation, the velocity of the fluid flow and the thermal expansion of the injected fluid which coupled with a JTC (Joule–Thomson cooling) temperature lowering.

2.4.1. Heat conduction and convection

In this sub-section, the energy conservation equation is derived to account for the gas expansion through heat convection and conduction processes. The equation that describes heat transfer by convection and conduction reads

$$\frac{\partial(C_{eq}T)}{\partial t} + \underbrace{\nabla \cdot (-K_{eq}\nabla T)}_{\text{Conduction}} = \underbrace{-C_L\mu \cdot \nabla T}_{\text{Convection}} + \underbrace{\alpha_T T \frac{\partial p}{\partial t} + \alpha_T T\mu \cdot \nabla p}_{JTC} + Q_H + Q_G \quad (15)$$

In this equation, C_{eq} denotes the effective volumetric heat capacity; K_{eq} defines the effective thermal conductivity; and C_L is the volumetric heat capacity of the moving fluid. The second and third terms on the right-hand side of the equation are related to JTC, Joule–Thomson cooling (Obinna and Horne, 2008; Singh et al., 2011); Q_H and Q_G denote general and geothermal heat sources, which can be spatially and temporally varying with other physics in the model.

Typically for the CO₂ sequestration in coal seams,

$$C_{eq} = (1 - \phi) \cdot \rho_s \cdot C_s + \phi \cdot \rho_L C_L \quad (16)$$

$$K_{eq} = K_L^\phi K_S^{(1-\phi)} \quad (17)$$

Here the subscripts 'L' and 's' denote the mobile fluid and solid properties, respectively.

The heat flux involves the heat transfer within and between immobile constituents as well as the moving fluid. The total heat flux is written as

$$N = -K_{eq}\nabla T + C_L u T \quad (18)$$

where N denotes the heat flux vector, and contains two terms. The first term describes heat flux in proportional to the temperature gradient and the second term is the convective flux moving at the liquid's bulk velocity.

2.4.2. Thermal boundary conditions

The boundary conditions are used to explain how the model domain interacts with the surrounding environment. The following thermal boundary conditions are commonly available:

- (a) *Temperature*: Specify a temperature on the boundary.
- (b) *Heat flux*: Specify the inward heat flux across the boundary.
- (c) *Convective flux*: This boundary condition represents a boundary where heat flows in and out with a fluid, applying in situations where the moving fluid carries the vast majority of heat and heat transfer is dominated by convection.
- (d) *Thermal insulation*: There is no heat flux across the boundary but temperature is allowed to change along it.
- (e) *Axial symmetry*: Use this boundary condition on the symmetry axis.

2.5. Temperature-dependent gas adsorption and thermal expansion

2.5.1. Langmuir adsorption

Several studies on Langmuir adsorption have shown that the monolayer amounts do vary with temperature. However, most of the experiments were performed at the same pressure range at different temperatures, and hence at higher temperatures, the isotherms represent less surface coverage. Sorptive surface coverage θ at a specific gas pressure decreases with increasing temperature as derived from thermodynamics. The sorption capacity also decreases with increasing temperature for the pressure range

that can be realized in laboratories (up to 50 MPa). This has been observed on sorption isotherms for dry coals (Croisdale et al., 2008; Lama and Bodziony, 1996; Levy et al., 1997; Sakurovs et al., 2008). However from thermodynamics the sorption capacity of a specific sample is similar for all temperatures at infinite gas pressures, assuming no change of the sample surface area over this temperature range. The impact of varying temperature on equilibrium constants like the Langmuir pressure p_L is given by the Van't Hoff equation (Busch and Gensterblum, 2011):

$$\left(\frac{\partial \ln p_L}{\partial (1/T)} \right)_\theta = \frac{-\Delta H}{R} \quad (19)$$

where H is the enthalpy of the system.

The variation of the Langmuir pressure p_L must be isosteric (at constant surface coverage θ). Like the energy, the enthalpy is a state function. The increase in enthalpy of a system is exactly equal to the energy added through heat, provided that the system is under constant pressure and that the only work done on the system is expansion work:

$$\Delta H = q \quad (20)$$

where q is the energy added to the system through heat.

The heat capacity at constant pressure is defined as

$$C_p = \left(\frac{\partial H}{\partial T} \right)_p \quad (21)$$

where C_p is the heat capacity at constant pressure.

The change in enthalpy for a range of temperature can be defined by integrating the heat capacity with respect to temperature,

$$\Delta H = \int_{T_1}^{T_2} C_p(T) dT \quad (22)$$

where T_1 and T_2 are the initial and final temperatures in the system.

The enthalpy ΔH is negative during the adsorption process, because sorption is an exothermic reaction. The surface coverage at constant gas pressure decreases with increasing temperature, however the magnitude of this decrease varies for all gases and depends on the sample/gas specific enthalpy of sorption. The gas with the highest sorption enthalpy will have the lowest decrease in sorption capacity.

The Langmuir pressure can be expressed with the of heat capacity as

$$\ln\left(\frac{p_L}{p_{L0}}\right)_\theta = \int_{T_0}^T \frac{\Delta H}{RT^2} dT = \frac{1}{R} \int_{T_0}^T \frac{1}{T^2} \int_{T_0}^T C_p(t) dt dT \quad (23)$$

By integrating Eq. (23), p_L can be expressed as a function of T as follows:

$$p_L = p_{L0} \exp\left(-\frac{C_p(T)(T - T_0)}{R} \left(\frac{1}{T} - \frac{1}{T_0}\right)\right), \quad p_L > p_{L0} \text{ if } T > T_0 \quad (24)$$

$$p_L = p_{L0} \exp\left(\frac{C_p(T)(T - T_0)}{R} \left(\frac{1}{T} - \frac{1}{T_0}\right)\right), \quad p_L < p_{L0} \text{ if } T < T_0 \quad (25)$$

Substituting Eqs. (24) and (25) into Eq. (5), the sorption-induced strain ε_s is then defined as a function of temperature.

2.5.2. Joule–Thomson cooling effect

CO₂ expands from high pressure to low pressure as it flows from the bottom hole to the coal reservoir; therefore, the potential energy of the gas increases since the intermolecular attraction increases as the distance between the adjacent molecular grows,

which inversely causes a decrease of the kinetic energy and temperature drop (Singh et al., 2011). In thermodynamics, the temperature change of a gas as it expands while no heat is exchanged with the environment is described by the Joule–Thomson process. The change in temperature depends not only on the initial and final pressure, but also the manner in which the expansion is carried out. In this research, since no heat is exchanged with the environment as CO₂ is injected into coal seams, the enthalpy of the system remains constant. The magnitude of temperature change during the cooling process is calculated through the Joule–Thomson coefficient, μ_{JT} , which describes the relationship between the change rate of temperature and pressure upon gas expansion in a steady state of flow with neither heat nor work done on the system.

$$\Delta T = \mu_{JT} \Delta p \quad (26)$$

Assuming there is only heat convection and JTC process during the CO₂ expansion, the energy conservation in steady state can be simplified as

$$C_L \mu \cdot \nabla T = \alpha_T T \mu \cdot \nabla p \quad (27)$$

By integration, the relationship between the temperature change and pressure change is derived.

2.6. Complete formulation of coupled THM model

The fully coupled thermal, hydrogeological and mechanical (THM) model is defined as a set of field Eqs. (1), (6), (14) and (15). Cross couplings between these field equations are illustrated in Fig. 1.

Fig. 1 illustrates the coupled THM processes in fractured coal seams. The coupling mechanisms for the hydro-mechanical processes are the interdependencies between the fracture aperture, coal porosity/permeability, fluid pressure and mechanical stress. The coupling link for thermo-mechanical processes is the volume expansion and thermal stress increment of the coal matrix due to the thermal gradient (and thus indirectly the fracture aperture change), and the conversion of dissipated mechanical work into thermal energy, which is usually negligible in practice but may be significant in geophysical and tectonic problems, such as the frictional heating induced by fault movements. The coupling links for thermo-hydraulic processes are more complex, involving variations in volume (density), viscosity and phase changes (such as evaporation and condensation) of the fluid phases by the thermal gradient, and the conductive–convective thermal transfer through fractured coal by the motion of fluids.

3. Complex evolution of coal permeability

The full formulation of coupled processes as defined above has been implemented into and solved by Comsol Multiphysics, a commercial partial differential equation solver. In this section, a series of numerical tests are conducted to evaluate the complex evolution of coal permeability during CO₂ injection. The goal is to explicitly simulate the dynamic interactions between coal matrix swelling/shrinking and fracture aperture alteration, and translate these interactions to permeability evolution under unconstrained swellings.

The selected geometry is a regular array of interacting cracks as shown in Fig. 2(b). The influence of effective stress and sorption-induced swelling response on a rectangular crack is examined. A single component part is removed from the array where the appropriate boundary conditions are applied as uniform displacement along the boundaries. This represents the symmetry of the displacement boundary condition mid-way between flaws as shown in Fig. 2(a). The simulation model geometry is 1.0 cm by 1.0 cm with

Table 1
Basic parameters for simulation cases.

Parameter	Value
Micro pore porosity (%)	5
Matrix permeability (m ²)	10 ⁻²²
Gas viscosity (Pa s)	1.2278 × 10 ⁻⁵
Young's modulus (GPa)	3.95
Poisson ratio	0.339
Biot's coefficient	0.66
Thermal expansion coefficient	9 × 10 ⁻⁵
Coal density (kg/m ³)	1500
Langmuir swelling strain	0.03
Langmuir sorption constant (m ³ /kg)	0.04316
Langmuir pressure p_L (MPa)	3.96
Confining pressure (MPa)	12
Initial temperature (K)	298.15
Universal gas constant (m Pa ³ /(mol K))	8.3144
Initial pressure (MPa)	0.1

a fracture located at the centre. The fracture is 3 mm in length and 0.2 mm in width.

Roller boundaries are applied on the left and bottom sides. The other two boundaries are stress controlled so that the matrix and the fracture could swell freely. No flow is applied for each flow boundary in four directions. No heat flux flows through any boundary but temperature is allowed to change since thermal insulation is applied on each boundary. CO₂ is injected with pressure of 10 MPa at temperature of 278.15 K into the coal seams with the initial pressure of 0.1 MPa and initial temperature of 298.15 K. The observed change of cleat aperture is due to the effective stress change which is the total effect of sorption-induced swelling and thermal contraction.

The input parameters for the simulations are detailed in Table 1 (Liu et al., 2011b). A time-dependent temperature is applied on the fracture boundary.

$$T_{bw}(t) = T_r + T_{in}(1 - e^{-(t/t_d)}) \quad (28)$$

where T_{bw} is the injection temperature; T_r is the initial temperature; T_{in} is the temperature increment due to injection. The time t_d is the characteristic time to control injection speed. The change rate in temperature is controlled by

$$\frac{dT_{bw}(t)}{dt} = \frac{T_{in}}{t_d} e^{-(t/t_d)} \quad (29)$$

It is difficult to keep $dT_{bw}(t)/dt$ constant but we can keep

$$\frac{T_{in}}{t_d} = C \quad (30)$$

The temperature will be kept constant after it reaches the injection value.

4. Results and discussions

4.1. Model validation

In our simulation model, the cleat permeability is calculated through the change of cleats aperture. Coal fracture permeability can be determined by fracture spacing and aperture (Liu et al., 1999).

Under the 2D case with two orthogonal sets of fractures, the directional permeability for different directions are defined as follows:

$$k_{fi} = \frac{b_j^3}{12 \cdot s}, \quad i \neq j \quad (31)$$

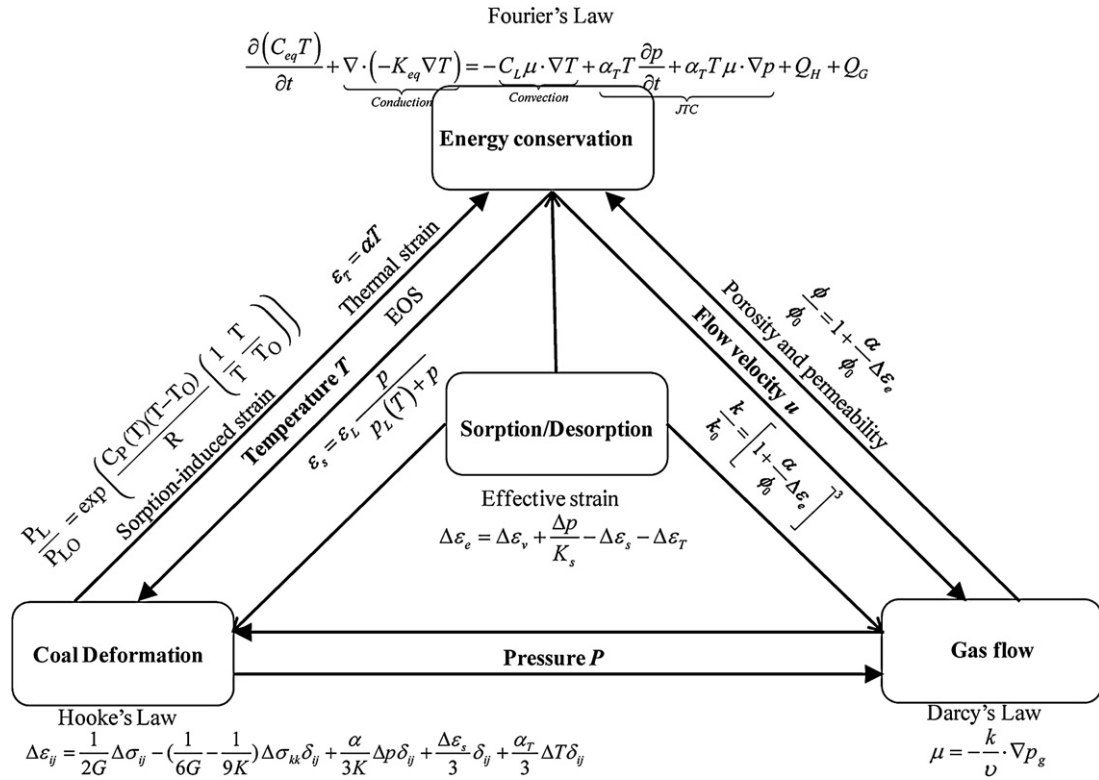


Fig. 1. Coupled relationships among coal deformation, gas flow, and thermal transport field equations.

where k_{fi} is cleat permeability of coal and b_j is the fracture aperture for i direction; s is the fracture spacing. Therefore, in the vertical direction,

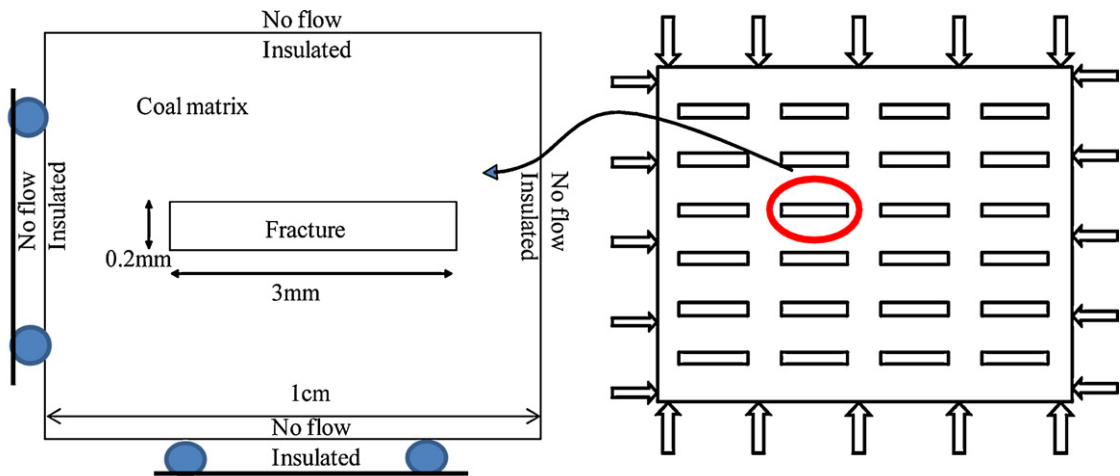
$$\frac{k_f}{k_{f0}} = \frac{(b + \Delta b)^3}{b^3} = \left(1 + \frac{\Delta b}{b}\right)^3 \quad (32)$$

where Δb is the change of cleat aperture, k_f is the cleat permeability and k_{f0} is the initial cleat permeability. At the final state, Δb is caused by 3 components, the scorpion-induced strain, thermal strain and the compressive strain.

$$\Delta b = \varepsilon_L \left(\frac{p}{p_L(T) + p} - \frac{p_0}{p_L(T_0) + p_0}\right) - \frac{\Delta p}{K_s} + \alpha_T \Delta T \quad (33)$$

As the coal swelling propagates from the vicinity of the cleat to the external boundary, the coal bridge swelling increases the cleat aperture while the matrix swelling changes the fracture spacing only. As $t = \infty$, the whole system gets equilibrium and the gas pressures in both coal cleats and matrix are the same and could be expressed as p . At the uniform swelling state, the permeability is only determined by the bridge swelling caused by the scorpion induced swelling and thermal expansion, since the term of $\Delta p/K_s$ is relatively small compared to the other 2 terms.

$$\frac{k_f}{k_{f0}}(t = \infty) = \left(1 + \varepsilon_L \left(\frac{p}{p_L(T) + p} - \frac{p_0}{p_L(T_0) + p_0}\right) - \frac{\Delta p}{K_s} + \alpha_T \Delta T\right)^3 \approx \left(1 + \varepsilon_L \left(\frac{p}{p_L(T) + p} - \frac{p_0}{p_L(T_0) + p_0}\right) + \alpha_T \Delta T\right)^3 \quad (34)$$



(a). Coal block with single matrix and fracture (b). Numerical model with stress-controlled boundary

Fig. 2. Specifications of the numerical model. (a) Coal block with single matrix and fracture. (b) Numerical model with stress-controlled boundary.

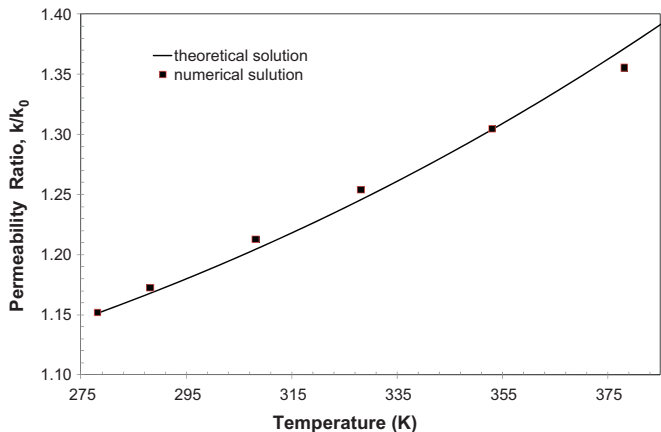


Fig. 3. Comparison of coal permeability ratio evolution at the equilibrium state between the theoretical solution and numerical solution.

In all modelling examples, the permeability at the initial and final state conditions is known. Comparison between modelled permeability at the equilibrium and the theoretical solution is shown in Fig. 3. The perfect match proves the validity of the modelling approach.

4.2. Permeability ratio evolution comparison between isothermal and non-isothermal cases

In this section, complex evolutions of coal permeability from the initial state to the final state are examined in a series of scenarios. The simulation results shown in Figs. 3–10 are based on the numerical model shown in Fig. 2(a). The permeability shown in these results are cleats permeability and they are calculated based on cubic law of single fracture.

Case 1. Isothermal CO₂ injection. In this scenario, it is assumed that the thermal equilibrium between the injected CO₂ and the coal matrix reaches instantly.

Evolutions of the coal permeability ratio under three different temperatures of 278.15 K, 328.15 K and 378.15 K are compared in Fig. 4. It is noticeable that the final permeability values on these 3 lines are the same after 10⁸ s. This indicates that permeability under these isothermal conditions becomes identical at the final states. However, the processes from the initial state to the final state are different due to the density discrepancy under different temperatures. According to the real gas law, gas density changes with pressure and temperature. The pressure evolutions are

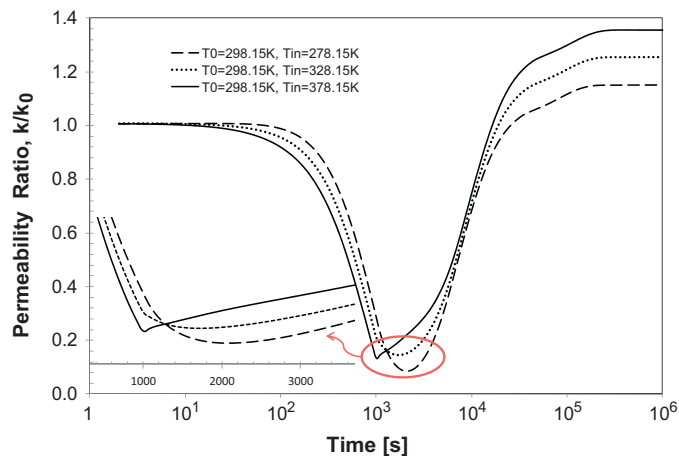


Fig. 5. Evolutions of permeability ratio under different non-isothermal conditions.

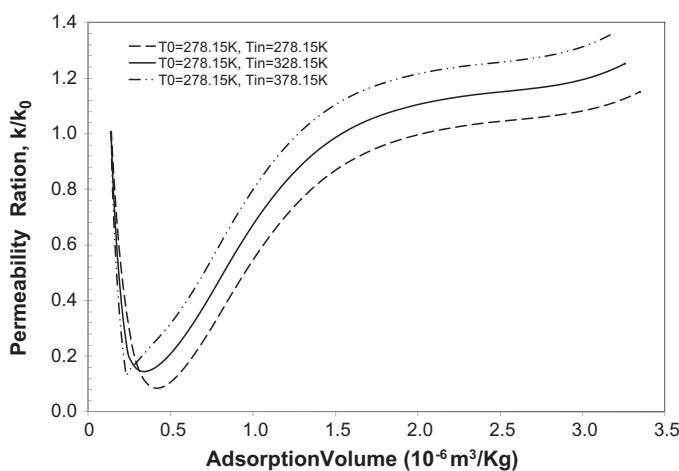


Fig. 6. Evolutions of permeability ratio with the amount of the adsorbed gas.

distinct under different temperatures, which affects the permeability evolutions. The permeability change of coal is determined by the compressibility and sorption-induced strain. In this scenario, both factors are controlled by pressure only under the isothermal conditions because thermal expansion effect is eliminated since there assumed to be no temperature difference between the injected CO₂ and the coal seams.

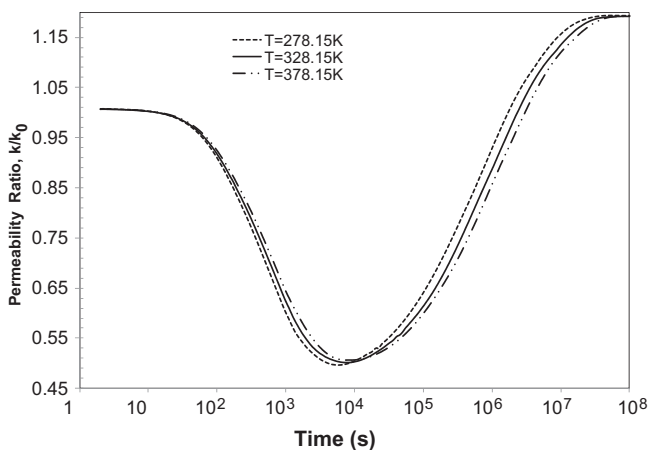


Fig. 4. Evolutions of isothermal permeability ratio under different temperatures.

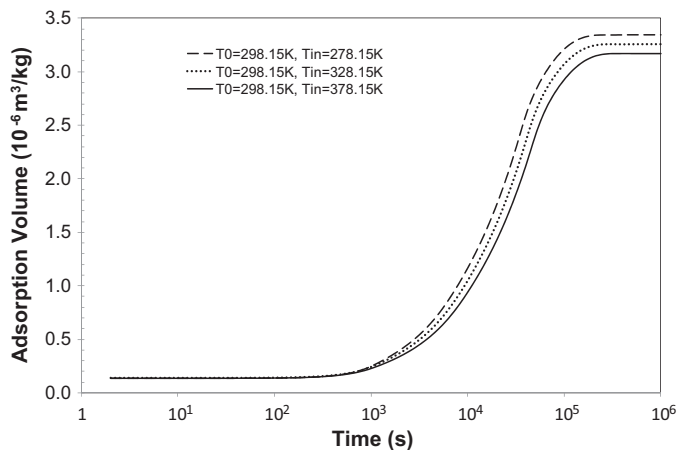


Fig. 7. Evolutions of the absolute adsorption capacity at different temperatures.

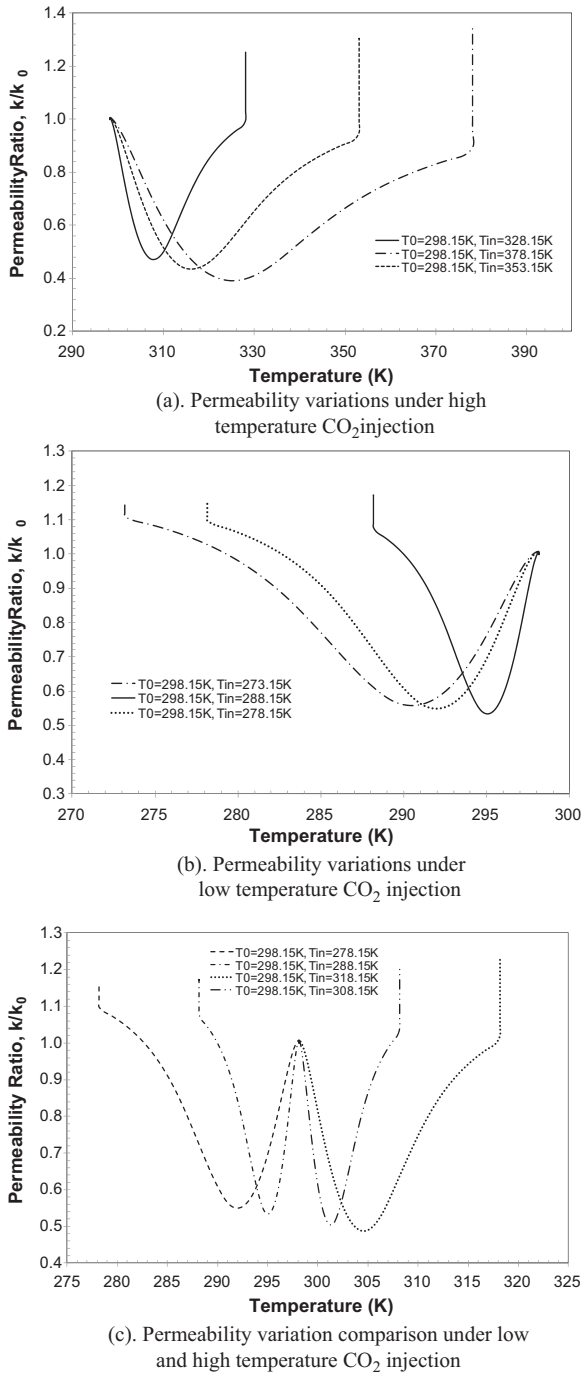


Fig. 8. Evolutions of coal permeability ratio with temperature. (a) Permeability variations under high temperature CO₂ injection. (b) Permeability variations under low temperature CO₂ injection. (c) Permeability variation comparison under low and high temperature CO₂ injection.

Case 2. Non-isothermal CO₂ injection. In this scenario, it is assumed that the thermal equilibrium between the injected CO₂ and the coal does not reach instantly.

Fig. 5 illustrates evolutions of the coal permeability ratio under three non-isothermal conditions as CO₂ is injected at the temperature of 278.15 K, 328.15 K and 378.15 K, respectively, into the coal seams with the initial temperature of 298.15 K. The trends of these three lines are similar but the differences are also noticeable.

The permeability for 3 cases decrease rapidly at the beginning, and then rebound after reaching the lowest value. However, the magnitudes and times for the switch of permeability from

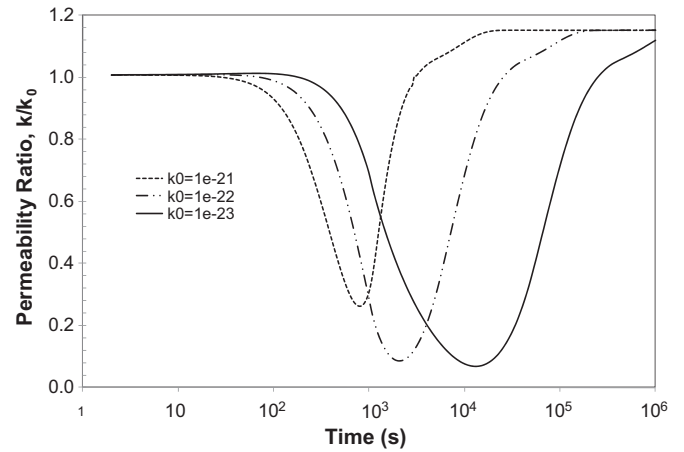


Fig. 9. Evolutions of coal permeability ratio at different initial permeabilities.

reduction to rebound at 278.15 K are apparently different from those at 378.15 K.

In these simulations, the maximum permeability reduction at the temperature of 278.15 K is 95% while it is 85% at the temperature of 378.15 K, and the final permeability recovers to 1.14 at the temperature of 278.15 K while the recovery at the temperature of 378.15 K is 1.35. Therefore, the permeability reduction at 378.15 K is 10% less and the recovery is 20% more than that at 278.15 K. The magnitude of permeability decrease at the temperature of 378.15 K is relatively small comparing to those at the other two temperatures, which is due to the balance between the sorption-induced strain and thermal strain in effective strain. The adsorption amount V_s decreases with the increase of temperature due to the increase of p_L . Since the sorption-induced volumetric strain is proportional to the volume of adsorption, the decrease of adsorption amount and increase of desorption amount at high temperature cause coal matrix to shrink and permeability to decrease less. On the other hand, the thermal strain increases with temperature, leading to the expansion of coal matrix and more permeability decrease. However, permeability decreases less at high temperature because of the dominant effect of sorption-induced strain in the effective strain.

The switching times are also different for these simulations. Permeability starts to change earlier but it takes longer time for the whole system to reach equilibrium at the temperature of 378.15 K. Permeability begins to decrease after 10 s of injection for the case of 378.15 K while it is not until 100 s that permeability start decreasing

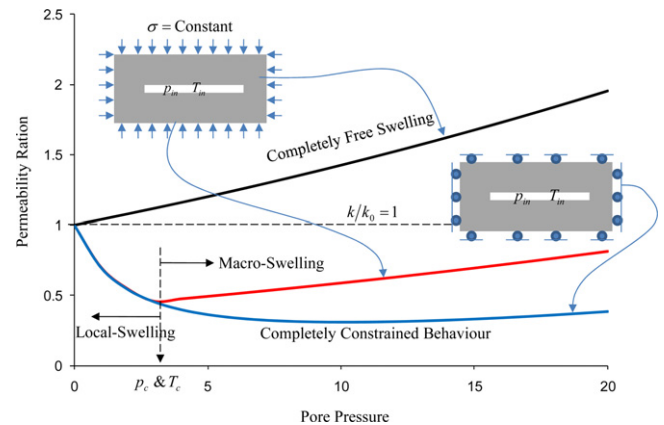


Fig. 10. Evolution of coal permeability during CO₂ non-isothermal injection as confined by two extreme cases: completely free swelling and completely constrained swelling.

for the case of 278.15 K. Moreover, permeability starts to rebound at 1000 s at the temperature of 378.15 K, but it is still decreasing for 278.15 K and 328.15 K at this time. Permeability starts to rebound at about 1600 s for the temperature of 328.15 K and at 2200 s for the temperature of 278.15 K. The system gets equilibrium almost at the same time for the 3 temperature cases. It is obvious that the permeability evolution time from rebound to equilibrium for the case of 378.15 K is the longest among these cases because the temperature difference between the injected CO₂ and the coal seams for the case of 378.15 K is over 50 K larger than those of the other two cases. In addition, the permeability switch from reduction to rebound is virtually instant at 378.15 K, while it takes more time and the lines are much smoother for the other 2 cases. Furthermore, permeability rebounds with a relatively small rate from 1000 s to 5000 s at the beginning of recovery for the case of 378.15 K, while it recovers with a larger rising rate at the temperature of 278.15 K as permeability starts to rebound after 2200 s. The recovery rate becomes almost the same at around 10⁴ s for all 3 temperature cases. The time difference seems not large among these 3 lines for this particular simulation model because this model is only designed to simulate one single fracture of 3 mm × 0.2 mm in a 1.0 cm × 1.0 cm tiny coal mess. However, there are numerous fractures and cleats in the coal reservoir and the time accumulation of the temperature effect is expected much larger than that in this model.

Comparing to the average evolution time of 10⁸ s from the initial state to the final state in the previous isothermal cases, it only takes approximately 5 × 10⁵ s for the non-isothermal injections to get equilibrium. Gas diffuses faster in the coal matrix under the non-isothermal condition due to the heat convection between the injected CO₂ and the coal, which accelerates the gas flow and shortens the time for the whole system to get equilibrium (Shi et al., 2008). Normally the switch from permeability reduction to recovery is very quick as the injection temperature is high. The transitional period for the case of 378.15 K is shorter than that for the case of 278.15 K since the coal permeability is higher for the case of 378.15 K and gas flows faster from the coal cleat to and within the coal matrix while the permeability is lower for the case of 278.15 K and gas flows slower.

Both the amount of gas that adsorbs in the coal and the flow rate that gas diffuses from the cleat to and within the coal matrix affect the magnitude of the coal matrix swelling and the rate of permeability change. Permeability decreases with the increase of injection pressure under the isothermal conditions due to the swelling of coal matrix caused by the adsorption of CO₂ in coal. However, the reason for the permeability decrease under non-isothermal condition is more complicated because apart from the effect of pressure, temperature causes the coal volume to change as well, which works through thermal expansion and gas adsorption. Thermal expansion leads to coal swelling at high temperature and thermal contraction leads to coal shrinking at low temperature, whereas, the effect of temperature on gas adsorption is more significant. Since gas adsorption capacity decreases with increasing temperature, more gas adsorbs on the coal at low temperature while more gas desorbs from the coal at high temperature. As a result, the magnitude of sorption-induced coal matrix swelling at low temperature is larger than that at high temperature. However, the gas diffusion rate increases with increasing temperature, and gas diffuses faster at high temperature which accelerates the permeability changing rate. Therefore, permeability variation induced by temperature is not caused by a sole factor but the result of multi-factors controlling both sorption-induced swelling and thermal expansion.

4.3. Permeability and adsorption amount

Inaccuracies in temperature readings and their effects on sorption measurements have been reported and discussed frequently in

the literature. Temperature errors are commonly between 0.1 and 0.3 K for experimental temperatures well above room temperature. This is because it is typically easier to heat a system than to cool it and to keep it at a constant temperature. Therefore, experimental temperatures below room temperature are expected to have a larger uncertainty. Evidently this effect is almost negligible for CH₄ (<0.1%). For CO₂ however it is quite significant and exhibits a maximum around the critical pressure of CO₂ where small temperature changes cause large changes in CO₂ density (Busch and Gensterblum, 2011).

In a typical isothermal experiment, CO₂ is injected from the injection pump to the coal sample. It is observed that temperature experiences several fluctuations until the gas adsorption gets equilibrium. Temperature decreases at the beginning as CO₂ is injected from the injection pump to the coal sample due to the cooling effect caused by gas expansion from the high pressure to the low pressure. The Joule–Thomson cooling process and the viscous heat dissipation with a temperature decrease depend strongly on the medium porosity. CO₂ is kept injected until the gas pressure in the coal sample reaches the same as the injection pressure. After the injection is stopped, gas pressure in the coal sample decreases dramatically in a very short time because of the adsorption of CO₂. CO₂ adsorbs on the large macro pores at the first place and changes from free phase to adsorbed phase. The pressure decrease slows down after the large pores are almost occupied and CO₂ begins to adsorb on the medium and micro pores. Meanwhile, temperature increases gradually with the gas adsorption since the adsorption process is an exothermic process and the large amount of heat released to the system leads to a slow recovery of the gas pressure after the adsorption gets equilibrium. Whereas, the adsorption and desorption processes always happen simultaneously. The exothermic adsorption and the endothermic desorption balance the temperature in the whole system through the entire process.

Based on such observations, permeability actually varies considerably during the adsorption process. However, the current permeability measurement method does not involve any dynamic adsorption process. Permeability is only determined by the analysis of the gas flow through the sample caused by the differential pressure decay between the upstream and downstream vessels after the adsorption gets equilibrium. Therefore, this kind of permeability measurement could not reflect the real permeability evolution under the effect of coal matrix swelling caused by pressure and temperature changes during the adsorption process.

In this paper, permeability ratio is investigated with respect to the adsorption amount. Permeability decreases dramatically in a short time at the first stage of adsorption because the adsorbed CO₂ on the surface of cleats and large pores of the coal directly narrows the path for the gas flow and reduces the permeability. The permeability decrease rate is larger as CO₂ is injected for the case of 378.15 K than those for other cases, as shown in Fig. 6, and a 10% less decrease is observed as permeability reaches the lowest point. The flow and adsorption rate of the gas is affected by the temperature of injected CO₂ as well as the temperature difference between the injected CO₂ and the coal matrix under the same injection pressure. The magnitude of permeability decrease at this adsorption stage is also related to the cooling effect. In fact, it is demonstrated that the cooling effect on the low temperature CO₂ injection is much larger than that on the high temperature CO₂ injection especially on those injections with the temperature around the freezing point of water because the solid hydrate may block the cleats as well as the pores, substantially reducing the permeability.

The second stage of the adsorption on the medium and small micro pores slows down due to the small gas diffusivity from the cleats to and within the coal matrix. Permeability switches from reduction to recovery with the increase of the adsorption amount because the matrix swelling switches correspondingly

from local swelling around the coal cleats to the global swelling within the whole coal matrix. The magnitude of adsorption amount where permeability starts to recover is different at varied injection temperatures under the same injection pressure. Permeability begins to switch from reduction to recovery as $2.5 \times 10^{-7} \text{ m}^3/\text{kg CO}_2$ adsorbs on the coal surface for the case of 378.15 K, while it does not rebound until $5 \times 10^{-7} \text{ m}^3/\text{kg CO}_2$ adsorbs on the coal surface for the case of 278.15 K, doubling the amount of adsorption for the case of 378.15 K. In addition, the magnitude of permeability at the switch point for the case of 378.15 K is 10% higher than that for the case of 278.15 K and the 10% higher permeability is kept through the whole recovery process until the adsorption reaches equilibrium. However, there is an obvious inflexion in the period of recovery for all three cases. Permeability rebounds sharply with a large increasing rate right after the switch point and then smooths as it almost reaches the initial value where the increase slows down until the permeability reaches the final value. The rate of permeability recovery is highly related to the extent of coal matrix swelling, which diminishes at high temperature due to the decreasing adsorption capacity with increasing temperature, as shown in Fig. 7. However, thermal expansion at high temperature causes the coal to swell and enhances the coal swelling. Consequently, the magnitude and rate of permeability recovery are the balance of these two temperature dependent mechanisms.

4.4. Permeability variation with temperature

In this section, the relationship between permeability and temperature is illustrated in terms of high temperature CO₂ injection and low temperature CO₂ injection. CO₂ is injected at three different temperatures of 328.15 K, 353.15 K and 378.15 K respectively for the high temperature injection case and at 273.15 K, 278.15 K and 288.15 K for the low temperature injection case. The permeability evolutions against the various temperatures are shown in Fig. 8. Prior to the CO₂ injection, temperature of the coal seams remains at the initial temperature of 298.15 K. As CO₂ is injected, temperature in the vicinity of the cleats soon reaches the same as that of the injected CO₂, leading to a large temperature difference between the cleats and the coal matrix around. As a result, heat transfer in terms of heat conduction and convection occurs as gas diffuses from the cleat to coal matrix, but temperature in the coal matrix always lags that in the cleats.

In the following we analyse the results of high temperature and low temperature injection cases as shown in Fig. 8. At the initial stage, high temperature gas adsorbs on the cleat surface and diffuses in the vicinity of the cleat leading to local swelling. Permeability experiences a rapid decrease for each injection case because the cleat aperture reduces. This swelling-caused permeability decrease is controlled by the internal cleat boundary. However, the magnitudes of permeability decrease are different due to various temperature differences. With gas diffusing through the coal matrix, the temperature difference between the injected CO₂ and the coal seams reduces and the matrix swells from the internal cleat boundary through the whole matrix to the far away boundary, resulting in the increase of the cleat aperture and permeability switching from reduction to recovery. It is noticeable that the period of permeability reduction is much shorter than that of the recovery at each injection temperature since temperature increase in the coal matrix is much slower due to the low diffusivity of gas flow. As shown in Fig. 8(a), sheer permeability switch is observed for the case of relatively low temperature of 328.15 K while the switch is much placid for the case of 378.15 K because the larger the temperature difference, the longer time it takes for heat transfer. Similarly, for the low temperature CO₂ injection, sharp permeability switch can be noticed for the case of relatively high temperature of 288.15 K, as shown in Fig. 8(b), while the switch is

much smoother for the case of CO₂ injection at 273.15 K. The high temperature CO₂ injection at 308.15 K and 318.15 K are compared with low temperature CO₂ injection at 278.15 K and 288.15 K in Fig. 8(c). Permeability decreases 44% and recovers to 1.14 for the case of 278.15 K while it decreases as much as 52% and recovers to 1.22 at the temperature of 318.15 K. It is noticeable that for the same temperature difference between the injected CO₂ and the coal, high temperature CO₂ injection causes more permeability decrease for the local swelling and more permeability recovery for the global swelling.

4.5. The effect of initial permeability on low temperature CO₂ injection

Fig. 9 illustrates the effect of initial permeability on the magnitude of permeability change. CO₂ is injected at the temperature of 278.15 K into the coal seams of 298.15 K with the initial matrix permeability of 10^{-21} m^2 , 10^{-22} m^2 and 10^{-23} m^2 respectively. It is noticeable that the maximum cleat permeability decrease is 72% in the coal seams with an initial matrix permeability of 10^{-21} m^2 and it takes 10^4 s for the whole system to get equilibrium. However, for the coal with an initial matrix permeability of 10^{-23} m^2 , it takes as long as 10^6 s , virtually 100 times longer for the permeability to get equilibrium and a 20% more maximum permeability decrease is observed. In addition, the time from permeability reduction to recovery is much longer in the coal seams with lower initial permeability because gas diffuses very slowly from the cleats to the coal matrix and it takes more time for the swelling transfers from local to global. In the field CO₂ injection, low temperature CO₂ injection has more significant effect on the coal seams with low initial permeability. The temperature decrease caused by the injection has the potential to freeze the coal water and other liquids, easily blocking the coal pores and cleats, reducing the coal permeability and finally affecting the injectivity. Therefore, for the low permeability coal seams, low temperature CO₂ injection is more difficult and the final amount of injection is less due to the decrease of injectivity.

4.6. Model evaluation

Liu et al. (2011b) evaluated the performance of major coal permeability models against analytical solutions for the two extreme cases of either completely free swelling or completely constrained swelling. For the case of completely free swelling none of the swelling strain contributes to the change in coal permeability because effective stresses do not change. Conversely, for the case of completely constrained swelling the full swelling strain contributes to the change in coal permeability because the coal is completely constrained from all directions. Therefore, these two solutions represent the lower bound and the upper bound behaviours of permeability evolution, respectively.

The pressure and temperature have mutual effects on permeability as CO₂ is injected with high pressure under non-isothermal conditions. Thermal expansion could be analogous to the effect of the sorption-induced strain due to its effect on the coal swelling. For the case of completely free swelling, the coal permeability is determined by the change in pore pressure only

$$\frac{k}{k_0} = \left[1 + \frac{\alpha}{\phi_0} \left(\frac{\Delta p}{K} \right) \right]^3 \quad (35)$$

However, for the case of completely constrained swelling, the coal permeability is determined by the resultant sorption strain and thermal strain

$$\frac{k}{k_0} = \left[1 - \frac{\alpha}{\phi_0} \left(\frac{\varepsilon_L p}{p + p_L(T)} - \frac{\varepsilon_L p_0}{p_0 + p_L(T_0)} + \alpha_T \Delta T \right) \right]^3 \quad (36)$$

The change in temperature affects permeability through both adsorption capacity and thermal expansion. The solutions for these two cases are illustrated in Fig. 10.

Prior to the CO₂ injection, the temperature and pressure in the cleat are the same as those in the coal matrix. At the early stage of CO₂ injection, the temperature and pressure in the cleat reach the injection temperature and pressure almost instantly, which yields large temperature and pressure gradients between the cleat and coal matrix.

When the injection temperature is higher than the initial one, both the gas diffusion and the thermal diffusion cause coal matrix to swell in the vicinity of the coal cleat, and reduce permeability. As the processes progress, the swelling region propagates further into the matrix, the impact of swelling on the coal permeability diminishes and coal matrix swelling changes from local swelling to global swelling. The change in temperature can also affect permeability through its effect on the adsorption capacity. The decrease of the adsorption capacity caused by the increasing temperature leads to the shrinking of the coal matrix. This partially offsets the effect of sorption-induced swelling and thermal expansion. Consequently, the permeability evolution becomes more uncertain.

5. Conclusions

A fully coupled coal deformation, gas flow, and thermal transport model is developed to evaluate the complicated evolution of coal permeability under the combined influence of variable gas pressure and temperatures. These combined effects are evaluated through explicit simulations of the dynamic interactions between coal matrix swelling/shrinking and fracture aperture alteration, and translations of these interactions to the evolution of coal permeability. In our formulations, we include the influence of temperature on sorption capacity via the temperature dependent Langmuir pressure and modify the conventional Langmuir adsorption equation. The effect of thermal stress, thermal expansion on permeability and the effect of temperature on coal matrix swelling are taken into account and coupled with the gas flow and coal deformation. The fully coupled model is applied to evaluate why coal permeability changes instantaneously from reduction to enhancement under the free swelling condition as widely reported in the literature. Based on the modelling results, the complex evolution of coal permeability under variable pressure and temperatures is controlled primarily by the following factors:

- *Distribution of coal fractures*: Coal is a typical dual porosity/permeability system containing porous matrix surrounded by fractures. Our results demonstrate that the matrix–fracture interactions control the complex evolution of coal permeability under the influence of pressure and temperature. This influence is regulated by the external boundary conditions.
- *External boundary conditions*: Our results demonstrate that the transition of coal matrix swelling from local swelling to macro-swelling controls the simultaneous switching of coal permeability from the initial reduction to the late recovery. At the initial stage of CO₂ injection under variable temperatures, matrix swelling due to gas sorption, thermal expansion and the change in adsorption capacity is localized within the vicinity of the fracture compartment. As the injection continues, the swelling zone is widening further into the matrix and the swelling becomes macro-swelling. When the swelling is localized, coal permeability is controlled by the internal fracture boundary condition and behaves volumetrically; when the swelling becomes macro-swelling, coal permeability is controlled by the external boundary condition.
- *Coal swelling/shrinking*: The evolution of coal matrix swelling/shrinking is the primary process that controls the

evolution of coal permeability under the influence of variable pressure and temperatures. The variation in temperature affects coal permeability via thermal expansion and sorption-induced swelling. The thermal expansion caused by high temperature CO₂ injection enhances the coal matrix swelling while the decreased sorption capacity due to the increase of temperature reduces the magnitude of coal swelling.

Acknowledgements

This work is partially funded by the Chinese Scholarship Council and the Australia–China Natural Gas Technology Partnership Fund through scholarships. These supports are gratefully acknowledged.

References

- Bai, M., Elsworth, D., 2000. Coupled Processes in Subsurface Deformation, Flow and Transport. ASCE Press, 336 pp.
- Bear, J., Corapcioglu, M.Y., 1981. A mathematical model for consolidation in a thermoelastic aquifer due to hot water injection or pumping. *Water Resources Research* 17, 723–736.
- Busch, A., Gensterblum, Y., 2011. CBM and CO₂-ECBM related sorption processes in coal: a review. *International Journal of Coal Geology* 87 (2), 49–71.
- Charrière, D., Pokryszka, Z., Behra, P., 2010. Effect of pressure and temperature on diffusion of CO₂ and CH₄ into coal from the Lorraine basin (France). *International Journal of Coal Geology* 81, 373–380.
- Chen, Z., Liu, J., Elsworth, D., Connell, L.D., Pan, Z., 2010a. Impact of CO₂ injection and differential deformation on CO₂ injectivity under in situ stress conditions. *International Journal of Coal Geology* 81, 97–108.
- Chen, Z., Liu, J., Pan, Z., Connell, L., Elsworth, D., 2010b. Relations between coal permeability and directional strains and their application to San Juan Basin. In: 44th U.S. Rock Mechanics Symposium and 5th U.S.–Canada Rock Mechanics Symposium. American Rock Mechanics Association, Salt Lake City, UT.
- Chen, Z., Pan, Z., Liu, J., Connell, L.D., Elsworth, D., 2011. Effect of the effective stress coefficient and sorption-induced strain on the evolution of coal permeability: experimental observations. *International Journal of Greenhouse Gas Control* 5 (5), 1284–1293.
- Chilingar, G.V., 1964. Relationship between porosity, permeability, and grain-size distribution of sands and sandstones. In: Straaten, L.M.J.U.v. (Ed.), *Developments in Sedimentology*. Elsevier, pp. 71–75.
- Clarkson, C.R., Bustin, M., 2010. Coalbed Methane: Current Evaluation Methods, Future Technical Challenges, SPE Unconventional Gas Conference. Society of Petroleum Engineers, Pittsburgh, Pennsylvania, USA.
- Connell, L.D., 2009. Coupled flow and geomechanical processes during gas production from coal seams. *International Journal of Coal Geology* 79, 18–28.
- Connell, L.D., Detournay, C., 2009. Coupled flow and geomechanical processes during enhanced coal seam methane recovery through CO₂ sequestration. *International Journal of Coal Geology* 77, 222–233.
- Crosdale, P.J., Moore, T.A., Mares, T.E., 2008. Influence of moisture content and temperature on methane adsorption isotherm analysis for coals from a low-rank, biogenically-sourced gas reservoir. *International Journal of Coal Geology* 76, 166–174.
- Cui, X., Bustin, R.M., 2005. Volumetric strain associated with methane desorption and its impact on coalbed gas production from deep coal seams. *AAPG Bulletin* 89, 1181–1202.
- Day, S., Fry, R., Sakurovs, R., Weir, S., 2010. Swelling of Coals by Supercritical Gases and Its Relationship to Sorption. *Energy & Fuels* 24, 2777–2783.
- Deishad, M., Thomas, S.G., Wheeler, M.F., 2009. Parallel numerical reservoir simulations of non-isothermal compositional flow and chemistry. In: *SPE Reservoir Simulation Symposium Proceedings*, The Woodlands, TX.
- Donald, L., 1978. Uranium solution-mineral equilibria at low temperatures with applications to sedimentary ore deposits. *Geochimica et Cosmochimica Acta* 42 (6, Part A), 547–569.
- Durucan, S., Edwards, J.S., 1986. The effects of stress and fracturing on permeability of coal. *Mining Science and Technology* 3 (3), 205–216.
- Elsworth, D., 1989. Thermal permeability enhancement of blocky rocks: one-dimensional flows. *International Journal of Rock Mechanics and Mining Sciences* 26 (3–4), 329–339.
- Elsworth, D., Bai, M., 1992. Flow-deformation response of dual porosity media. *Journal of Geotechnical Engineering* 118 (1), 107–124.
- Gu, F., Chalaturnyk, J.J., 2005a. Analysis of coalbed methane production by reservoir and geomechanical coupling simulation. *Journal of Canadian Petroleum Technology* 44 (10), 33–42.
- Gu, F., Chalaturnyk, R.J., 2005b. Sensitivity study of coalbed methane production with reservoir and geomechanical coupling simulation. *Journal of Canadian Petroleum Technology* 44 (10), 23–32.
- Gu, F., Chalaturnyk, R.J., 2006. Numerical simulation of stress and strain due to gas sorption/desorption and their effects on in situ permeability of coalbeds. *Journal of Canadian Petroleum Technology* 45 (10), 52–62.
- Harpalani, S., Chen, G., 1997. Influence of gas production induced volumetric strain on permeability of coal. *Geotechnical and Geological Engineering* 15, 303–325.

- Harpalani, S., Schraufnagel, R.A., 1990. Shrinkage of coal matrix with release of gas and its impact on permeability of coal. *Fuel* 69, 551–556.
- Izadi, G., Wang, S., Elsworth, D., Liu, J., Wu, Y., Pone, D., 2011. Permeability evolution of fluid-infiltrated coal containing discrete fractures. *International Journal of Coal Geology* 85 (2), 202–211.
- Krooss, B.M., van Bergen, F., Gensterblum, Y., Siemons, N., Pagnier, H.J.M., David, P., 2002. High-pressure methane and carbon dioxide adsorption on dry and moisture-equilibrated Pennsylvanian coals. *International Journal of Coal Geology* 51 (2), 69–92.
- Lama, R.D., Bodziony, J., 1996. *Outbursts of Gas, Coal and Rock in Underground Coal Mines*. Westonprint Kiama, NSW, ISBN 0 646 29902 6.
- Levy, J.H., Day, S.J., Killingley, J.S., 1997. Methane capacities of Bowen basin coals related to coal properties. *Fuel* 76 (9), 813–819.
- Liu, J., Elsworth, D., Brady, B.H., 1999. Linking stress-dependent effective porosity and hydraulic conductivity fields to RMR. *International Journal of Rock Mechanics and Mining Sciences* 36 (5), 581–596.
- Liu, H.H., Rutqvist, J., 2010. A New coal-permeability model: internal swelling stress and fracture-matrix interaction. *Transport in Porous Media* 82, 157–171.
- Liu, J., Chen, Z., Elsworth, D., Miao, X., Mao, X., 2010a. Evaluation of stress-controlled coal swelling processes. *International Journal of Coal Geology* 83, 446–455.
- Liu, J., Chen, Z., Elsworth, D., Miao, X., Mao, X., 2010b. Linking gas-sorption induced changes in coal permeability to directional strains through a modulus reduction ratio. *International Journal of Coal Geology* 83, 21–30.
- Liu, J., Chen, Z., Elsworth, D., Qu, H., Chen, D., 2011a. Interactions of multiple processes during CBM extraction: a critical review. *International Journal of Coal Geology*, <http://dx.doi.org/10.1016/j.coal.2011.06.004>.
- Liu, J., Wang, J., Chen, Z., Wang, S., Elsworth, D., Jiang, Y., 2011b. Impact of transition from local swelling to macro swelling on the evolution of coal permeability. *International Journal of Coal Geology* 88 (1), 31–40.
- Long, Q.M., Wen, G.C., Zou, Y.H., Zhao, X.S., 2009. Experimental study on gas permeability by adsorption under 3D-stress. *Journal of Coal Science and Engineering (China)* 15, 148–151.
- Mazumder, S., Wolf, K.H., 2008. Differential swelling and permeability change of coal in response to CO₂ injection for ECBM. *International Journal of Coal Geology* 74 (2), 123–138.
- Nowacki, W., 1995. *Dynamic Problems of Thermoelasticity*. Noordhoff, Leiden, The Netherlands.
- Obinna, D., Horne, R.N., 2008. Modelling reservoir temperature transients and matching to permanent downhole gauge data for reservoir parameter estimation. In: *Proceedings of the SPE International Petroleum Conference and Exhibition, Denver, CO (Paper No. 115791-MS)*.
- Oldenburg, C.M., 2007. Joule-Thomson cooling due to CO₂ injection into natural gas reservoirs. *Energy Conversion and Management* 48 (2007), 1808–1815.
- Palmer, I., Mansoori, J., 1996. How permeability depends on stress and pore pressure in coalbeds: a new model. In: *SPE Annual Technical Conference and Exhibition, 1996 Copyright 1996, Society of Petroleum Engineers, Inc., Denver, CO*.
- Pan, Z., Connell, L.D., 2007. A theoretical model for gas adsorption-induced coal swelling. *International Journal of Coal Geology* 69, 243–252.
- Pan, Z., Connell, L.D., Camilleri, M., 2010. Laboratory characterisation of coal reservoir permeability for primary and enhanced coalbed methane recovery. *International Journal of Coal Geology* 82, 252–261.
- Pini, R., Ottiger, S., Burlini, L., Storti, G., Mazzotti, M., 2009. Role of adsorption and swelling on the dynamics of gas injection in coal. *Journal of Geophysical Research* 114, B04203.
- Qu, H.Y., Liu, J.S., Pan, Z.J., Connell, L., 2010. Impact of thermal processes on CO₂ injectivity into a coal seam. *IOP Conference Series: Materials Science and Engineering* 10 (1), 012090.
- Robertson, E.P., 2005. Modeling permeability in coal using sorption-induced strain data. In: *SPE Annual Technical Conference and Exhibition, Society of Petroleum Engineers, Dallas, TX*.
- Robertson, E.P., Christiansen, R.L., 2007. Modeling laboratory permeability in coal using sorption-induced strain data. *SPE Reservoir Evaluation & Engineering* 10, 260–269.
- Sakurovs, R., Day, S., Weir, S., Duffy, G., 2008. Temperature dependence of sorption of gases by coals and charcoals. *International Journal of Coal Geology* 73, 250–258.
- Saunders, R.T., Yang, J.T., 1985. Adsorption of gases on coals and heat-treated coals at elevated temperature and pressure: 1. Adsorption from hydrogen and methane as single gases. *Fuel* 64 (5), 616–620.
- Seidle, J.R., Huit, L.G., 1995. Experimental measurement of coal matrix shrinkage due to gas desorption and implications for coal permeability increases. In: *International Meeting on Petroleum Engineering, 1995 Copyright 1995, Society of Petroleum Engineers, Inc., Beijing, China*.
- Shi, J.Q., Durucan, S., 2004a. A numerical simulation study of the Allison unit CO₂-ECBM pilot: the impact of matrix shrinkage and swelling on ECBM production and CO₂ injectivity. In: *Proceedings of 7th International Conference on Greenhouse Gas Control Technologies*.
- Shi, J.Q., Durucan, S., 2004b. Drawdown induced changes in permeability of coalbeds: a new interpretation of the reservoir response to primary recovery. *Transport in Porous Media* 56, 1–16.
- Shi, J.Q., Mazumder, S., Wolf, K.H., Durucan, S., 2008. Competitive methane desorption by supercritical CO₂ injection in coal. *Transport in Porous Media* 75 (1), 35–54.
- Singh, A.K., Goerke, U.J., Kolditz, O., 2011. Numerical simulation of non-isothermal compositional gas flow: application to carbon dioxide injection into gas reservoirs. *Energy* 36 (5), 3446–3458.
- Siriwardane, H., Haljasmaa, I., McLendon, R., Irdi, G., Soong, Y., Bromhal, G., 2009. Influence of carbon dioxide on coal permeability determined by pressure transient methods. *International Journal of Coal Geology* 77, 109–118.
- Somerton, W.H., Söylemezoglu, I.M., Dudley, R.C., 1975. Effect of stress on permeability of coal. *International Journal of Rock Mechanics and Mining Sciences & Geomechanics Abstracts* 12 (5–6), 129–145.
- Wang, G.X., Wei, X.R., Wang, K., Massarotto, P., Rudolph, V., 2010. Sorption-induced swelling/shrinkage and permeability of coal under stressed adsorption/desorption conditions. *International Journal of Coal Geology* 83 (1), 46–54.
- Wang, S., Elsworth, D., Liu, J., 2011. Permeability evolution in fractured coal: the roles of fracture geometry and water-content. *International Journal of Coal Geology* 87, 13–25.
- Wu, Y., Liu, J., Elsworth, D., Chen, Z., Connel, L., Pan, Z., 2010a. Dual poroelastic response of a coal seam to CO₂ injection. *International Journal of Greenhouse Gas Control* 4 (4), 668–678.
- Wu, Y., Liu, J., Elsworth, D., Miao, X., Mao, X., 2010b. Development of anisotropic permeability during coalbed methane production. *Journal of Natural Gas Science and Engineering* 2 (4), 197–210.
- Wu, Y., Liu, J., Chen, Z., Elsworth, D., Pone, D., 2011. A dual poroelastic model for CO₂-enhanced coalbed methane recovery. *International Journal of Coal Geology* 86 (2–3), 177–189.
- Zhang, H., Liu, J., Elsworth, D., 2008. How sorption-induced matrix deformation affects gas flow in coal seams: a new FE model. *International Journal of Rock Mechanics and Mining Sciences* 45, 1226–1236.
- Zhou, Y., Rajapakse, R.K.N.D., Graham, J., 1998. A coupled thermoporoelastic model with thermo-osmosis and thermal-filtration. *International Journal of Solids and Structures* 35, 4659–4683.
- Zhu, W.C., Wei, C.H., Liu, J., Qu, H.Y., Elsworth, D., 2011. A model of coal-gas interaction under variable temperatures. *International Journal of Coal Geology* 86 (2–3), 213–221.